











Expanding the Time Domain of Multiple Populations: Evidence of Nitrogen Variations in the ~ 1.5 Gyr Old Star Cluster NGC 1783

Mario Cadelano^{1,2} , Emanuele Dalessandro² , Maurizio Salaris^{3,4} , Nate Bastian^{3,5,6} , Alessio Mucciarelli^{1,2} , Sara Saracino³ , Silvia Martocchia⁷ , and Ivan Cabrera-Ziri⁸ 

¹ Dipartimento di Fisica e Astronomia “Augusto Righi,” Università degli Studi di Bologna, Via Gobetti 93/2, I-40129 Bologna, Italy; mario.cadelano@unibo.it

² INAF-Osservatorio di Astrofisica e Scienze dello Spazio di Bologna, Via Gobetti 93/3, I-40129 Bologna, Italy

³ Astrophysics Research Institute, Liverpool John Moores University, 146 Brownlow Hill, Liverpool L3 5RF, UK

⁴ INAF—Osservatorio Astronomico d’Abruzzo, via M. Maggini, I-64100, Teramo, Italy

⁵ Donostia International Physics Center (DIPC), Paseo Manuel de Lardizabal, 4, E-20018 Donostia-San Sebastián, Guipuzkoa, Spain

⁶ IKERBASQUE, Basque Foundation for Science, E-48013, Bilbao, Spain

⁷ Department of Astrophysics/IMAPP, Radboud University, P.O. Box 9010, 6500 GL Nijmegen, The Netherlands

⁸ Astronomisches Rechen-Institut, Zentrum für Astronomie der Universität Heidelberg, Mönchhofstraße 12-14, D-69120 Heidelberg, Germany

Received 2021 November 9; revised 2021 December 10; accepted 2021 December 10; published 2021 December 31

Abstract

We present the result of a detailed analysis of Hubble Space Telescope UV and optical deep images of the massive and young (~ 1.5 Gyr) stellar cluster NGC 1783 in the Large Magellanic Cloud. This system does not show evidence of multiple populations (MPs) along the red giant branch (RGB) stars. However, we find that the cluster main sequence (MS) shows evidence of a significant broadening (50% larger than what is expected from photometric errors) along with hints of possible bimodality in the MP sensitive ($m_{F343N} - m_{F438W}$, m_{F438W}) color–magnitude diagram (CMD). Such an effect is observed in all color combinations including the m_{F343N} filter, while it is not found in the optical CMDs. This observational evidence suggests we might have found light-element chemical abundance variations along the MS of NGC 1783, which represents the first detection of MPs in a system younger than 2 Gyr. A comparison with isochrones including MP-like abundances shows that the observed broadening is compatible with a N abundance enhancement of $\Delta([N/Fe]) \sim 0.3$. Our analysis also confirms previous results about the lack of MPs along the cluster RGB. However, we find that the apparent disagreement between the results found on the MS and the RGB is compatible with the mixing effects linked to the first dredge up. This study provides new key information about the MP phenomenon and suggests that star clusters form in a similar way at any cosmic age.

Unified Astronomy Thesaurus concepts: Star clusters (1567); Photometry (1234); Globular star clusters (656); Large Magellanic Cloud (903); Stellar populations (1622)

1. Introduction

Globular clusters (GCs) exhibit star-to-star variations in their light-element content (e.g., Carretta et al. 2009). In fact, while some GC stars have the same light-element abundances as the field at the same metallicity (first population—FP), others show enhanced N and Na along with depleted C and O abundances (second population—SP). Such anomalies are readily observable also by using color–magnitude diagrams (CMDs) involving specific near-UV filters sensitive to OH, CN, and CH molecular bands (e.g., Sbordone et al. 2011; Piotto et al. 2015). The manifestation of such light-element inhomogeneities is referred to as multiple populations (MPs). A number of scenarios have been proposed over the years to explain the formation of MPs (e.g., Decressin et al. 2007; D’Ercole et al. 2008; Denissenkov & Hartwick 2014; Gieles et al. 2018), however, their origin is still strongly debated (see Bastian & Lardo 2018; Gratton et al. 2019 for a recent review).

The MP phenomenon appears to be ubiquitous. In fact, not only all massive and old Galactic GCs host MPs (e.g., Piotto et al. 2015; Milone et al. 2017), but MPs are also observed in the Large and Small Magellanic Cloud (LMC, SMC) old stellar

clusters (Mucciarelli et al. 2009; Dalessandro et al. 2016), in GCs in dwarf galaxies such as Fornax (Larsen et al. 2014), and in the M31 GC systems (Schiavon et al. 2013), and there are strong indications (though based on integrated quantities) that they are a common property of stellar clusters in massive elliptical galaxies (e.g., Chung et al. 2011). Conversely, several works based on photometric and spectroscopic analysis of red giant branch stars (RGBs—e.g., Mucciarelli et al. 2008, 2014; Martocchia et al. 2018) suggest that massive clusters younger than ~ 2 Gyr do not show any inhomogeneity in their light-element content. In fact, NGC 1978 in the LMC is the youngest cluster ($t \sim 2$ Gyr) found to host subpopulations with light-element chemical variations so far (Martocchia et al. 2018; Saracino et al. 2020a). It is worth stressing that, while young clusters (< 2 Gyr) do show features in their optical CMDs (e.g., extended main-sequence turnoffs, dual main sequences) that are not consistent with the classical notion of a simple stellar population, these features are not due to abundance variations (Mucciarelli et al. 2008, 2009) but are likely due to stellar rotation (Bastian & de Mink 2009; Kamann et al. 2020, 2021). Hence, while they may be in principle related to MPs, the underlying cause is different.

The lack of MPs in young (< 2 Gyr) clusters is completely unexpected and inconsistent with predictions for all theories of MP formation. We note also that an age of 2 Gyr corresponds to a formation redshift of $z = 0.17$, well past the peak epoch of GC formation (e.g., Brodie & Strader 2006). One possible

explanation for the lack of MPs in young age (<2 Gyr) clusters is that old GCs were simply much more massive at birth than those systems that do not show abundance spreads. Such large masses may allow GCs to retain stellar ejecta of stars within them and also to accrete pristine gas from their surroundings. Indeed, cluster mass is found to play a significant role in shaping the properties of MPs in GCs (Carretta et al. 2010; Milone et al. 2017). One alternative explanation is that light-element variations also exist within young clusters, but they are difficult/impossible to observe along the RGB, where they have been typically searched for. In fact, Salaris et al. (2020) have recently shown that the mixing effect associated with the first dredge up can have a differential impact on the surface chemical abundances of FP and SP RGB stars and it is able to smooth out their initial N abundance differences with increasing efficiency for decreasing ages.

To finally establish the presence of MPs in young massive clusters, it is therefore key to search for MPs along their main sequence (MS). To this aim, we have started a comprehensive study of the young (~ 1.5 Gyr, Mucciarelli et al. 2007; Zhang et al. 2018) cluster NGC 1783 in the LMC. This system represents an optimal choice in this context as it is quite massive ($\sim 2 \times 10^5 M_{\odot}$; Song et al. 2021), it is located in a region of the LMC characterized by low extinction ($A_V < 0.1$ mag) and by a negligible field contamination. In addition, previous photometric and spectroscopic studies of RGB stars (Mucciarelli et al. 2007; Cabrera-Ziri et al. 2016; Martocchia et al. 2018, 2021; Zhang et al. 2018) suggest that this cluster does not host MPs. Here we present the results of the first detailed screening of the cluster MS obtained through deep Hubble Space Telescope (HST) optical and UV MP sensitive photometry.

The Letter is structured as follows. In Section 2 the adopted data set and data-reduction procedures are described. Section 3 reports on the MP analysis in the CMD and a comparison with theoretical models. Finally we discuss the main results in Section 4.

2. Observations and Data Analysis

2.1. Data Set and Data Reduction

This work is based on observations obtained with the UVIS channel of the Wide Field Camera 3 (WFC3) and the Advanced Camera for Surveys (ACS) aboard HST. The main data set is composed of proprietary WFC3 data obtained under GO 16255 (PI: E. Dalessandro) and consists of 8 images acquired with the F343N filter (6×3086 s and 2×3095 s) and 6 images acquired with the F438W filter (6×938 s). These data were then combined with archival images obtained under GO 10595 (PI: P. Goudfrooij) and GO 12257 (PI: L. Girardi). These complementary data sets consist of 3 ACS images acquired with each of the following filters, F435W (2×340 s and 1×90 s), F555W (2×340 s and 1×40 s), F814W filter (2×340 s and 1×8 s) and 3 WFC3 images acquired with the F336W filter (2×1190 s and 1×1200 s).

The photometric analysis of the entire data set was performed by using DAOPHOT IV (Stetson 1987) and following the approach adopted in previous works (see Dalessandro et al. 2018a, 2018b; Cadelano et al. 2019, 2020a). Briefly, tens of bright and isolated stars have been selected in each frame to model the point-spread function (PSF), which has been eventually applied to all sources

detected in each image above 3σ , where σ is the standard deviation of the background counts. We then created a master list composed of stars detected in at least half of the deep F343N and F438W images. At the corresponding positions of stars in this final master list, a fit was forced with DAOPHOT/ALLFRAME (Stetson 1994) in each frame of the two data sets. For each star thus recovered, multiple magnitude estimates obtained in each chip were homogenized by using DAOMATCH and DAOMASTER, and their weighted mean and standard deviation were finally adopted as star magnitude and photometric error. The final catalog includes all the sources detected in at least two filters.

Instrumental magnitudes were calibrated using the equations and zero-points quoted in the dedicated instrument webpage.⁹ Magnitudes were then corrected for the effect of differential reddening following the approach described in Cadelano et al. (2020c; see also Dalessandro et al. 2018a and the Appendix for further details).

Instrumental positions were corrected for filter-dependent geometric distortions using the prescriptions by Anderson & King (2006), Bellini & Bedin (2009), and Bellini et al. (2011) and then converted into the absolute coordinate systems by using the stars in common with Saracino et al. (2020b) as a secondary astrometric reference frame.

The left panels of Figure 1 show the (m_{F438W} , $m_{F438W} - m_{F814W}$) and the (m_{F438W} , $m_{F343N} - m_{F438W}$) differential reddening corrected CMDs as an example.

2.2. Proper Motion Analysis

We took advantage of the large temporal baseline of ~ 15 yr spanned by the observations and obtained over 5 different epochs (i.e., 2006, 2011, 2016, 2019, and 2021) to perform a relative proper motion (PM) analysis and clean the cluster CMD from field interlopers. To derive the cluster's relative PMs, we followed the approach described in Dalessandro et al. (2013; see also Cadelano et al. 2017, Dalessandro et al. 2018b, and Massari et al. 2021). The procedure consists of measuring the instrumental position displacements of the stars detected in all the available epochs once a common distortion-free reference frame is defined. As a first step, we obtained a precise measurement of the mean stellar positions in each epoch by averaging their instrumental coordinates measured in each frame of each filter. A 3σ clipping rejection was applied to maximize the accuracy of the final measurements. We then used a six-parameter linear transformation to shift the average positions of all the stars to a master list reference frame, which is composed by a sample of likely cluster's member stars selected according to their position in the optical CMDs of the 2006 ACS observations. For each star, the master-frame transformed positions as a function of the epoch are fit with a least-squares straight line, the slope of which represents the star's PM. The fitting procedure is iterated after data rejection and σ clipping. After deriving the first-pass PM estimates, we repeated the entire procedure, refining the reference master list by selecting likely member stars according to their first-pass PMs.

To obtain a catalog of stars composed of high probability cluster's members, we first applied quite strict astrometric quality selection criteria. Specifically, following the

⁹ <https://www.stsci.edu/hst/instrumentation/wfc3/data-analysis/photometric-calibration>

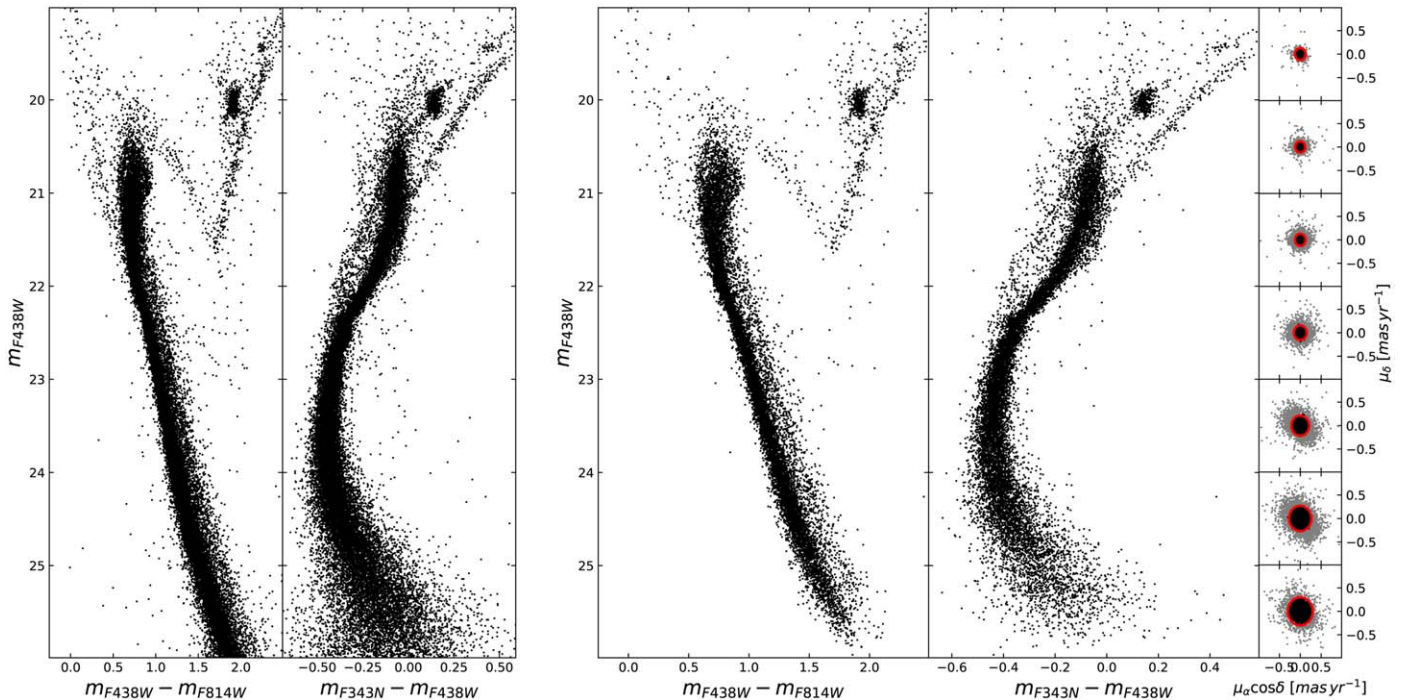


Figure 1. Left-hand panels: CMD of NGC 1783 in two different combination of filters as obtained from the entire catalog of stars. Magnitudes are corrected for differential reddening. Right-hand panels: same CMD as in the left-hand panels but only for PM selected stars. The right-hand panels show the VPD in different magnitude ranges: gray points represent all the stars with a PM measurement, the red circles enclose stars selected as bona fide cluster’s members, highlighted with black points.

prescriptions by Libralato et al. (2019) we selected (i) stars for which the reduced χ^2 of the PM fit is smaller than 2 in both components, (ii) stars having a PM fit based on at least three different epochs, (iii) stars having a PM error smaller than 3σ (where σ is the local standard deviation of the PM errors calculated over 0.5 large F438W magnitude bins). Then, to select bona fide cluster’s members we analyzed the vector-point diagrams (VPDs) in different magnitude bins in the range $19 < m_{F438W} < 26$. In each VPD, we performed a Gaussian fit to both the PM components. Stars having a PM smaller than 1σ , where σ represents the best-fit Gaussian width, are marked as bona fide cluster’s members and they are shown in the VPDs on the right panels of Figure 1.

3. Results

To explore the presence of MPs along the cluster MS, we mainly exploited the F343N magnitudes, which have been shown to be quite effective in separating MPs (e.g., Martocchia et al. 2018; Cabrera-Ziri et al. 2020). In Figure 2 we show the expected behavior of three stellar models in three example color combinations. The reference model is a BaSTI-IAC isochrone (Hidalgo et al. 2018) of appropriate age for NGC 1783 ($t \sim 1.5$ Gyr), metallicity $[\text{Fe}/\text{H}] = -0.35$ (Mucciarelli et al. 2008), distance $(m - M)_0 = 18.45$, extinction $E(B - V) = 0.02$, and scaled-solar chemical mixture. Such an isochrone is representative of the FP chemical composition. The other two models were obtained by using a coeval isochrone calculated for the same metallicity, but with two different choices for the metal distribution, in which the elements C, N, and O follow the observed MP (anti-) correlations. Specifically, the mildly enhanced model was obtained assuming $[\text{C}/\text{Fe}] = -0.2$, $[\text{N}/\text{Fe}] = +0.3$ and $[\text{O}/\text{Fe}] = -0.1$, while the highly enhanced model was created assuming

$[\text{C}/\text{Fe}] = -0.2$, $[\text{N}/\text{Fe}] = +0.7$ and $[\text{O}/\text{Fe}] = -0.5$. In both models the total C + N + O abundance is constant. The calculation of the model atmospheres and fluxes has been performed as described in Hidalgo et al. (2018). Figure 2 shows that the $(m_{F343N} - m_{F438W})$ color is the most efficient combination to separate MS stars with different N abundances, in particular, those with a mild N enhancement. It is also evident that the effect of N enhancement on the $(m_{F343N} - m_{F438W})$ color becomes particularly significant for magnitude $m_{F438W} > 23$. The enhancement effect decreases but is still appreciable when the F343N filter is combined with other optical filters (see an example in the middle panel of Figure 2). On the contrary, as expected, the three models do not show any significant difference in the case of optical filter combinations (see the example of the $m_{F438W} - m_{F814W}$, m_{F438W} CMD on the right-hand panel of Figure 2).

The MP analysis was performed on stars with high photometric quality. First, we removed from the catalog stars having large photometric errors, χ^2 , and sharpness values. In particular, for each filter, we divided the observed magnitude range in 0.5 mag large bins and removed those stars having at least one of the above quantities larger than 1σ from the local median values. Then we removed photometric binaries from the sample. To do this, we selected in the optical diagram $(m_{F438W} - m_{F814W}, m_{F438W})$ MS stars in the magnitude range $21.5 < m_{F438W} < 26$. Then, we divided the sequence in 0.5 mag large magnitude bins where we evaluate the median and standard deviation of the color and removed all the 1.5σ outliers. This allows us to remove a large fraction of photometric binaries having relatively high mass ratios. The resulting sample is shown with black dots in Figure 3.

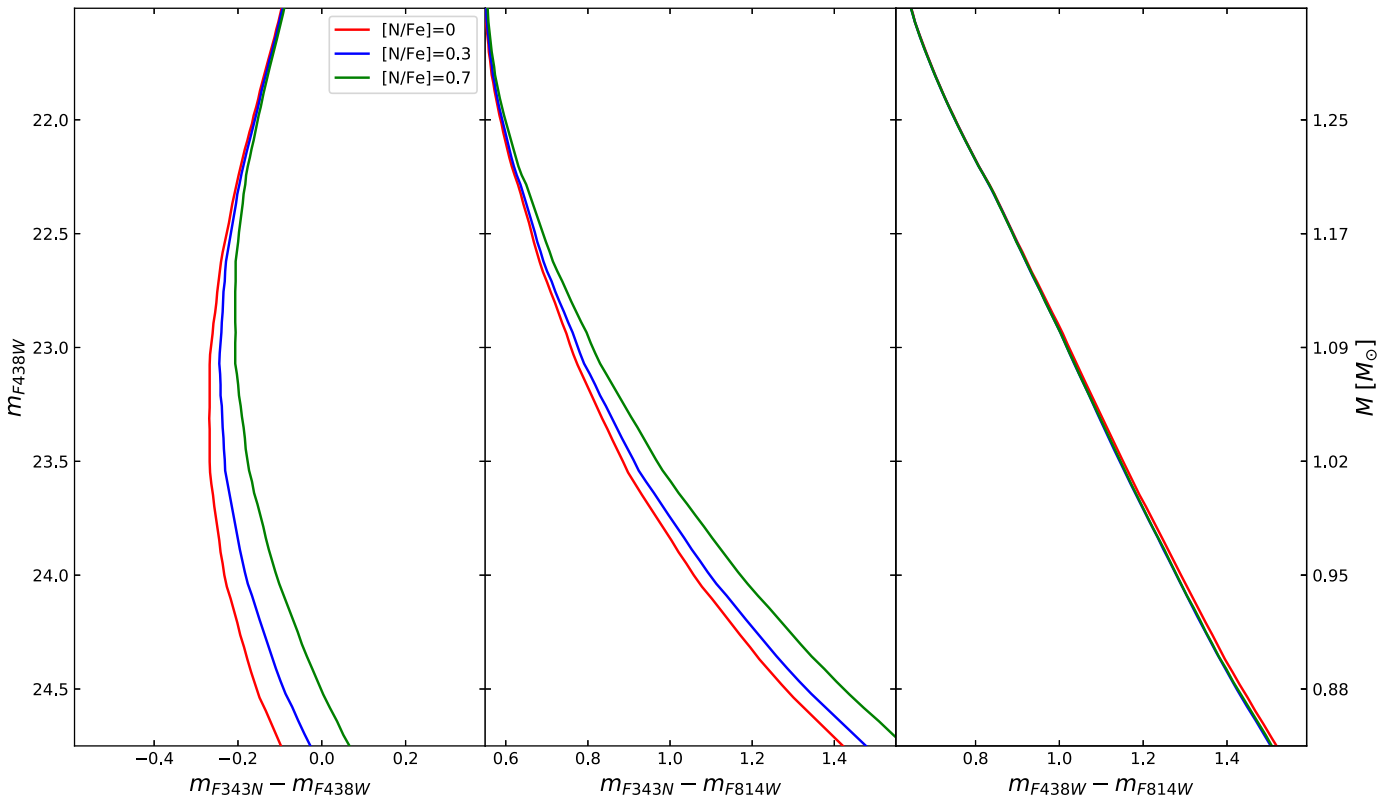


Figure 2. Isochrones of a ~ 1.5 Gyr stellar population with $[\text{Fe}/\text{H}] = -0.35$ and different N enrichment in the different filter combinations. The red, blue, and green curves represent a model with a solar-scaled composition, $[\text{N}/\text{Fe}] = 0.3$ and $[\text{N}/\text{Fe}] = 0.7$ mixture, respectively. The corresponding stellar masses are reported on the right-hand axis of the right-hand panel.

A first inspection of the CMDs in Figure 1 confirms the presence of an extended turnoff as commonly observed in young stellar systems and typically interpreted as due to stellar rotation. Such an effect progressively fades for increasing magnitudes and the MS reaches a minimum broadening at $m_{\text{F}438\text{W}} = 22.4$ (corresponding to a mass of $\sim 1.2 M_{\odot}$). Interestingly, for magnitudes $m_{\text{F}438\text{W}} > 22.4$ the MS width in the $(m_{\text{F}343\text{N}} - m_{\text{F}438\text{W}}, m_{\text{F}438\text{W}})$ diagram abruptly starts to grow again (Figure 3). We note that this effect is not observed in optical CMDs, but only when the F343N band is adopted and therefore it is plausible to exclude this as only due to photometric errors. In addition, we can also exclude this effect being due to a residual contamination by low-mass ratio unresolved binaries, as, given the almost vertical shape of the MS in the considered magnitude range in the $(m_{\text{F}343\text{N}} - m_{\text{F}438\text{W}}, m_{\text{F}438\text{W}})$ CMD, they are not expected to contribute significantly to the MS color distribution, while their effect would be more easily detectable in the optical CMDs. This points to a possible connection with the presence of MPs.

To assess quantitatively whether the observed MS broadening for $m_{\text{F}438\text{W}} > 22.4$ in the $(m_{\text{F}438\text{W}} - m_{\text{F}814\text{W}})$ combination can be explained in terms of photometric errors, we compared the observations with artificial stars. We performed a large number of artificial star test experiments following the prescriptions in Cadelano et al. (2020b, see also Dalessandro et al. 2015). We created a list of artificial stars with a F438W input magnitude extracted from a luminosity function modeled to reproduce the observed one and extrapolated beyond the limiting magnitude. Then, to each of these artificial stars, we assigned magnitudes in all the other available filters by interpolating along appropriate mean ridge lines. These artificial stars were added to the real

images by using the DAOPHOT/ADDSTAR software and by adopting a regular grid composed of 15×15 pixel cells (corresponding approximately to 10 times the typical FWHM of the point-spread function) in which only one artificial star for each run is allowed to lie. The photometric reduction process and the PSF models used for the artificial star experiments are the same as described in Section 2.1. This process was iterated multiple times. In the end, about 80,000 artificial stars are simulated for the entire field of view covered by the adopted data set. The same photometric quality selection criteria used for real stars were applied to the artificial stars.

We then compared the observed MS width with that derived from artificial star CMDs. To do this, we verticalized the distribution of MS stars with respect to two fiducial lines (see Dalessandro et al. 2018a, for a similar implementation of the technique) in the magnitude range $22.5 < m_{\text{F}438\text{W}} < 24.5$. We estimated the width of the verticalized color distributions by fitting them with a single Gaussian function. Results are shown in the right panels of Figure 3. Interestingly, we find that the observed MS is $\sim 50\%$ larger than the artificial one. A similar difference is measured also when other combinations of the F343N filter with optical filters, such as the F814W filter (see top panels of Figure 4), are considered. On the contrary, in all the color combinations including only optical filters, such as the $m_{\text{F}438\text{W}} - m_{\text{F}814\text{W}}$, $m_{\text{F}438\text{W}}$ CMD in the bottom panels of Figure 4, the observed verticalized distributions have only a 15%–20% larger widths than the artificial ones. It is important to stress that such an effect is commonly observed in these kinds of comparisons (see for example Dalessandro et al. 2011; Milone et al. 2012) and therefore cannot be considered as evidence of a significant difference.

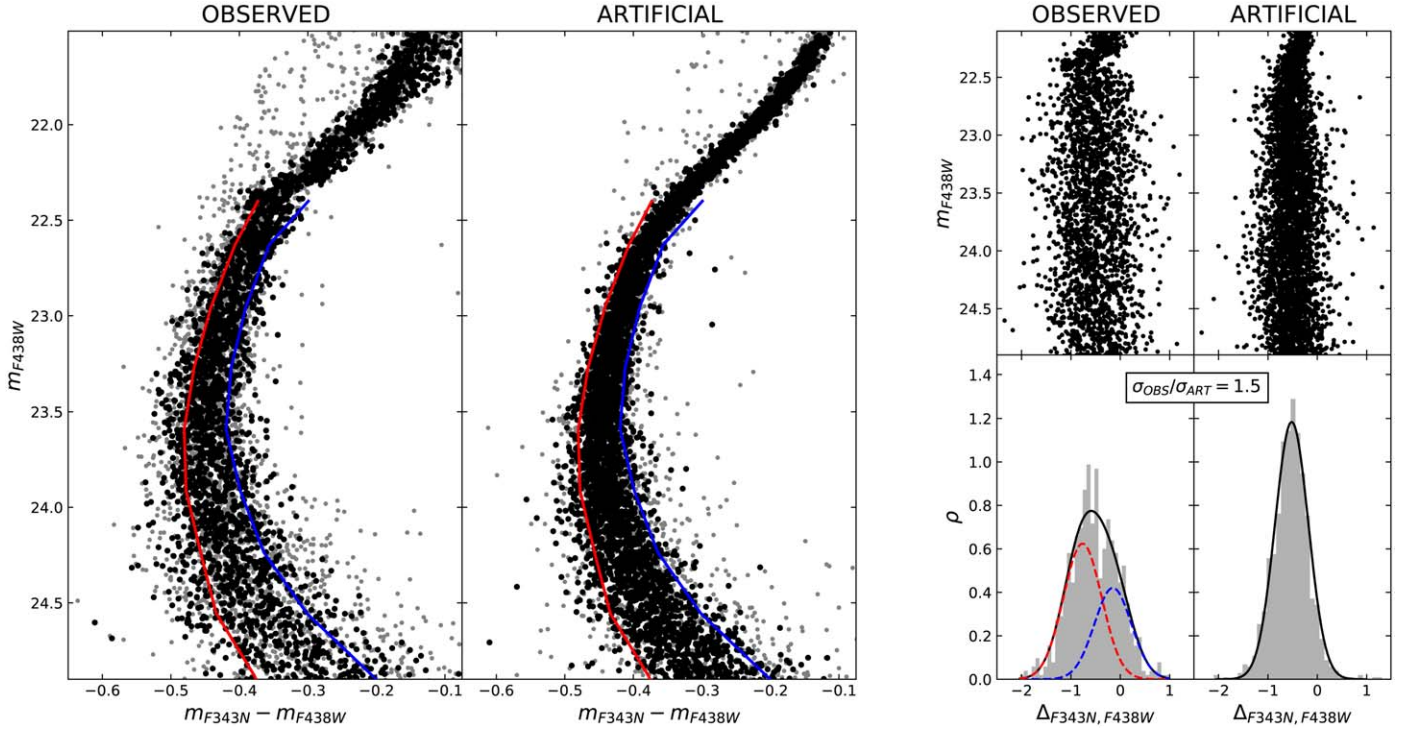


Figure 3. Left-hand panels: CMD of NGC 1783 in $(m_{F343N} - m_{F438W}, m_{F438W})$ filter combination of observed (left panel) and artificial stars (right panel). Black points are stars selected following the photometric and binary selection criteria explained in the text, while gray points are the stars that did not survive the selection. The blue and red curves are the fiducial lines adopted to verticalize the color distribution. Right-hand panels: the top panel displays the verticalized color distribution of MS stars (observed stars on the left, artificial stars on the right), while the bottom panel shows the corresponding histograms in the magnitude range $m_{F438W} = 23.75\text{--}24.5$. In the case of the observed stars, the two dashed curves are the two best-fit Gaussians while the solid black curve is their sum. In the case of artificial stars, the best single Gaussian fit is shown together with the ratio between the standard deviation of the observed (σ_{OBS}) and artificial (σ_{ART}) verticalized MSs.

This quantitative analysis suggests that the significant broadening along the MS of NGC 1783, observed only when UV filter N abundance sensitive combinations are considered, can represent the first detection of MPs in a massive stellar cluster younger than 2 Gyr.

Such observational evidence is further supported by the fact that the verticalized $(m_{F438W} - m_{F814W})$ color distribution (Figure 3) shows hints of bimodality. Indeed, in the observed star histogram in Figure 3 we can distinguish two distinct peaks with $\Delta_{F343N, F438W} \sim 1$ mag, that can be nicely fit by two Gaussian functions,¹⁰ whose width is compatible with that expected from photometric errors (i.e., their widths are compatible with that derived from artificial stars). We can exclude that such bi-modal distribution can be due to low-mass ratio unresolved binaries as they are expected to uniformly populate the MS color distribution in the considered range of magnitudes. Based on the expected distribution of MPs in this CMD (see Figure 2), the red Gaussian peak corresponds to the FP stars, and includes $\sim 60\%$ of the sample, while the bluer one corresponds to SP stars and includes the remaining $\sim 40\%$ of objects. We note that the presence of MPs along the MS becomes apparent in the magnitude range populated by stars with mass $M \leq 1 M_{\odot}$ (Figure 2). Finally, it is worth stressing that FP and SP stars are nicely separated in all color combinations including the F343N band, while they become indistinguishable when optical filter combinations are considered (Figure 5).

¹⁰ We used the Gaussian mixture model statistics (<https://scikit-learn.org/stable/index.html>) to perform the two component fit.

3.1. Comparison with Theoretical Models

To tentatively quantify the degree of N enrichment between FP and SP stars, we compared the observations with a set of synthetic CMDs mimicking a population composed of a mixture of stars having standard solar-scaled chemical composition and stars having a N enriched composition. To do so, we generated three different synthetic CMDs by populating the three isochrones shown in Figure 2. We divided the magnitude range $21.5 < m_{F438W} < 26$ in regular bins of 0.5 mag width. In each bin and for each isochrone we simulated 50 artificial stars by randomly extracting them from a uniform distribution in magnitude and from a normal distribution centered on the isochrone color and with a standard deviation equal to that measured from the artificial stars in the same magnitude bin. Here we assumed a flat luminosity function for the synthetic population and equally populated FP and SP. We note that results are basically unchanged if slightly different luminosity functions and population ratios are assumed. Results are shown in Figure 6.

The synthetic CMDs obtained by including stars with $[N/Fe] = 0.7$ (Figure 6) show either a clear split MS or a significantly larger ($>50\%$) broadening with respect to the observed CMD. On the contrary, we find that the synthetic CMD populated by a mixture of solar-scaled and $[N/Fe] = 0.3$ stars is able to nicely reproduce the observations. In fact, the resulting MS width differs by only $\sim 10\%$ from the observed one and the histogram of the verticalized distribution nicely matches the observed color distribution (Figures 3 and 6)—panel (a). This suggests that NGC 1783 hosts a

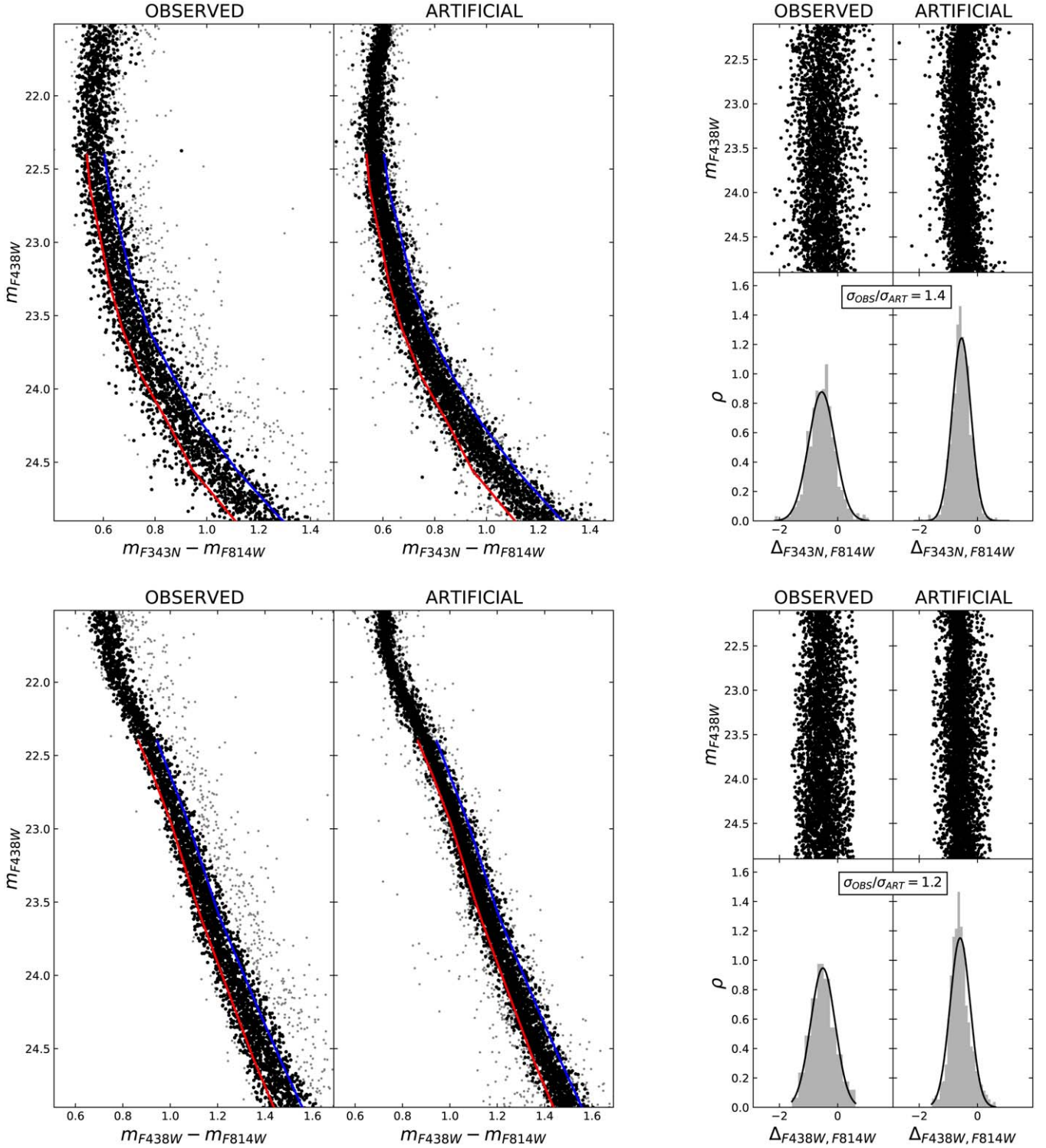


Figure 4. Top panels: same as in Figure 3 but in the case of the $(m_{F343N} - m_{F814W}, m_{F438W})$ filter combination. Bottom panels: same as in the top panels but in the purely optical $(m_{F438W} - m_{F814W}, m_{F438W})$ filter combination.

second population of stars moderately enriched in terms of N ($\Delta([N/Fe]) \sim 0.3$).

4. Discussion

The observational results presented in this Letter show that we have detected for the first time the presence of MPs differing in terms of their light-element abundances in a stellar

clusters younger than ~ 2 Gyr. These findings represent a potential major breakthrough in the field, as they would suggest, at odds with what has been found in the literature so far, that the MP phenomenon is common to all massive clusters, irrespective of their age. Hence, if GC formation is not a specific phenomenon of stellar systems formed at high- z , then GCs at any age can be used as a proxy to study the galaxy assembly processes (Kruijssen 2015; Horta et al. 2021).

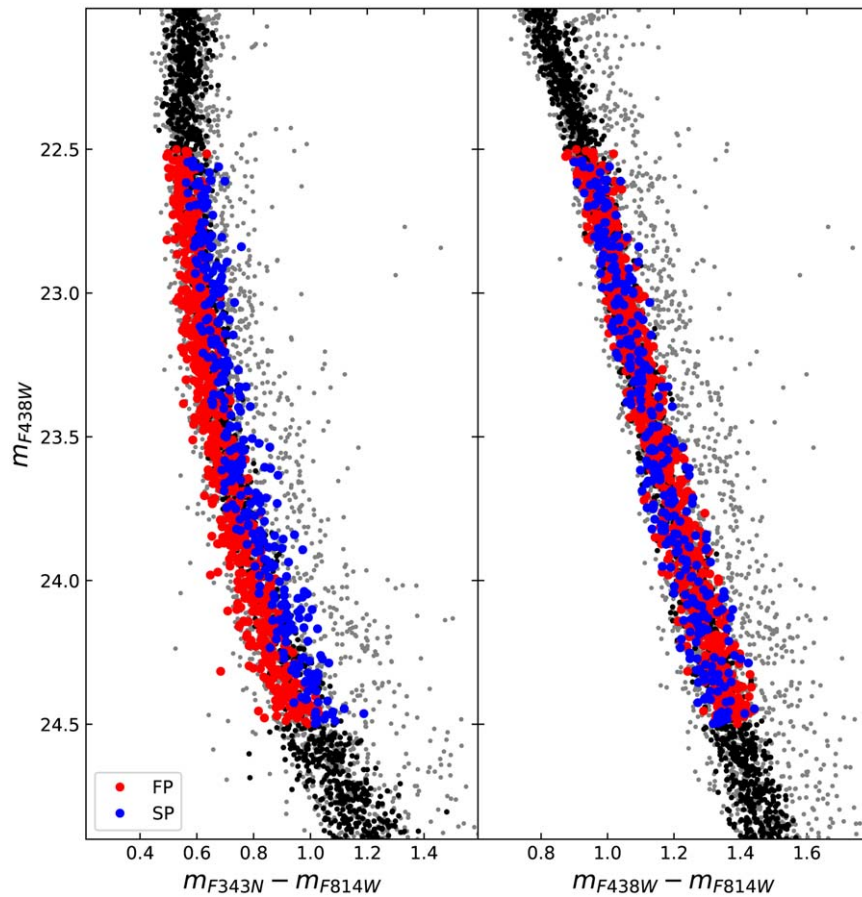


Figure 5. Left-hand panel: CMD of NGC 1783 in the filter combination ($m_{F343N} - m_{F814W}$, m_{F438W}). Black and gray points are the cluster’s members that survived and did not survive the photometric selection criteria. Red and blue dots are FP and SP stars selected on the basis of the bimodality presented in Figure 3. Right-hand panel: same as in the left-hand panel but in the purely optical filter combination ($m_{F438W} - m_{F814W}$, m_{F438W}).

Recently, Cabrera-Ziri et al. (2020) and Li et al. (2020) have carried out a similar study, looking for MPs on the MS of the massive ~ 1.5 Gyr old cluster NGC 419 in the SMC (see also the case of NGC 1846; Li 2021). The authors did not find any significant evidence of MPs in this cluster, however, their results might have been hampered by the quality of the available photometry (mainly due to the larger distance of the system) and therefore the cluster would deserve a follow-up analysis.

By comparing the observed CMDs with artificial stars and by following broadly the same approach used for the MS analysis, we confirm, based on more accurate photometry, previous findings about the lack of MPs along the cluster RGB. However, we estimate that the apparent disagreement between the results obtained for the RGB and MS is compatible with the expected mixing effects linked to the first dredge up. In fact, the results presented in Salaris et al. (2020) show that the mixing associated with the first dredge up can reduce the initial N differences among different subpopulations by a factor of about 2–3 at an age of ~ 1.5 Gyr. Therefore, in the specific case of NGC 1783, an initial spread of $\Delta[N/Fe] \sim 0.3$ dex, as constrained from the MS (Section 3.1), would be erased completely on the RGB, thus mimicking an homogeneous stellar population.

The combination of these results therefore suggests that to study MPs in very young systems it is necessary to focus on their MS, thus largely changing the observing strategies adopted so far. This calls for a dedicated study that would

reappraise our understanding of the MP phenomenon over cosmic time. It is interesting to note in this respect, that while this work shows that there is not a sharp age limit for the onset of MPs, nevertheless age can indeed play a role in shaping light-element chemical abundance variations. If we compare the initial N spread constrained from the MS of NGC 1783 ($\Delta(N/Fe) \sim 0.3$ dex) with what we found photometrically from the RGBs of intermediate-age and old clusters, after accounting for the effects of the first dredge up, we find indications of a possible correlation between cluster age and initial N spread with older clusters requiring an initial internal N variation of ~ 1 dex and the young ones a spread smaller by a factor ~ 5 (see Figure 6 in Salaris et al. 2020 and references therein). While it is necessary to investigate the significance of this trend further, one possibility is that it might be related to the initial cluster mass. In fact, while all clusters analyzed so far have comparable present-day masses ($M > 10^5 M_{\odot}$), older clusters could have been much more massive at birth than the younger ones. Larger masses may allow GCs to retain stellar ejecta more efficiently, and also accrete pristine gas from their surroundings. However, the notion that GCs lose a significant fraction of their initial mass or are able to accrete/retain significant amounts of gas is still strongly debated (e.g., Larsen et al. 2014; Bastian & Lardo 2015; Cabrera-Ziri et al. 2015; Dalessandro et al. 2019).

The results presented here also open the possibility of tightly constraining MP formation processes. For example, young star clusters can be used to detect the presence of age spread (not

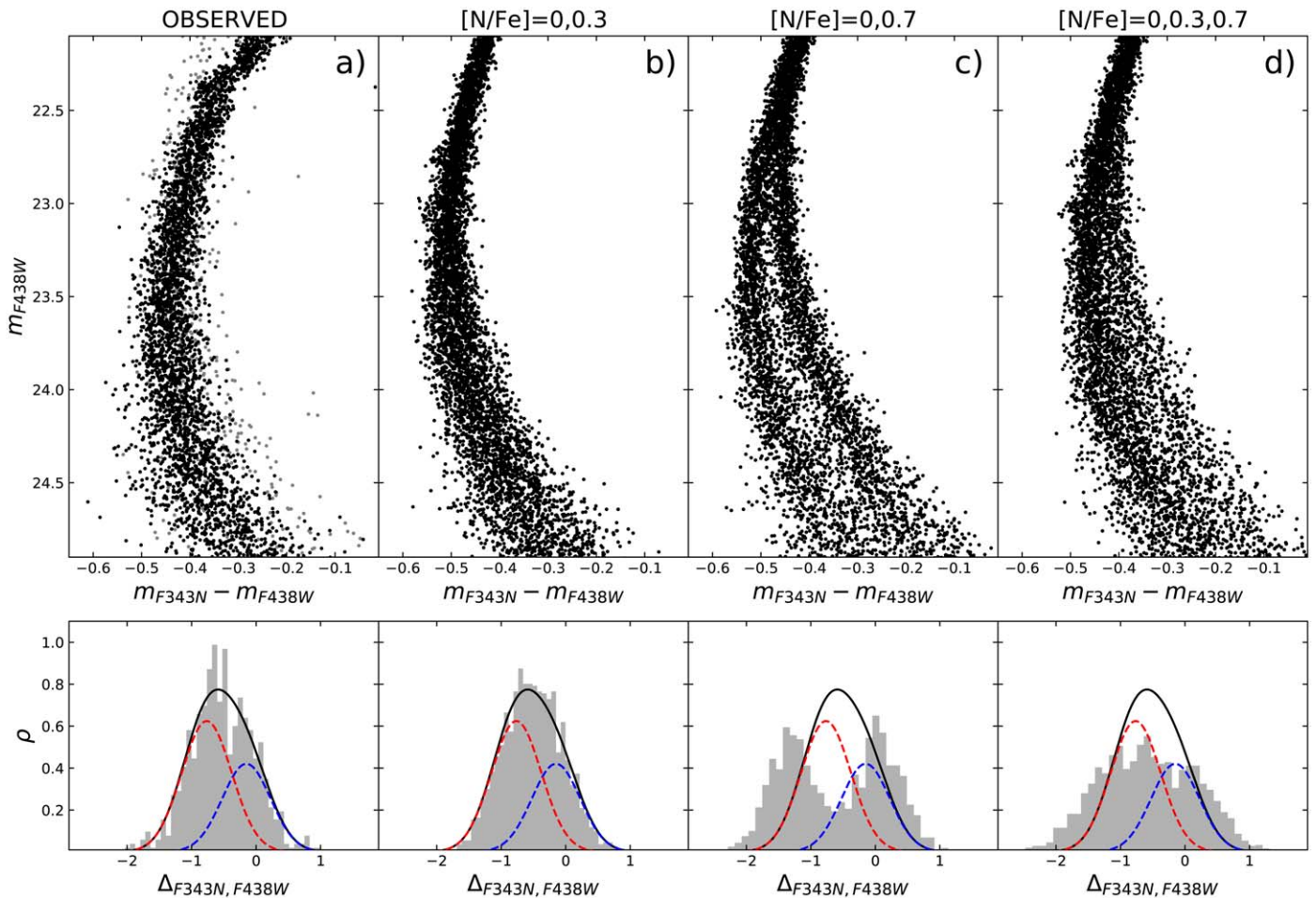


Figure 6. Panel (a): observed CMD in the $(m_{F343N} - m_{F438W}, m_{F438W})$ filter combination. Panel (b): synthetic CMD obtained with a mixture of $[N/Fe] = 0$ and $[N/Fe] = 0.3$ stars. Panel (c): same as in panel (b) but for a mixture of $[N/Fe] = 0$ and $[N/Fe] = 0.7$ stars. Panel (d): same as in panel (b) panel but for a combination of the three available mixtures. Bottom panels: histograms of the verticalized distributions of MS stars in the corresponding top panels. The blue, red, and black curves are the two Gaussian fits presented in Figure 3.

possible in the case of old clusters) which is one the major discriminators among MP formation models (e.g., Martocchia et al. 2018, 2019; Saracino et al. 2020a).

A detailed characterization of the MP properties in NGC 1783 requires a detailed spectroscopic follow-up. Given the distance of the system and faint magnitudes of the target stars, the use of integral field spectrographs and the application of the approach successfully adopted by Latour et al. (2019) and Saracino et al. (2020a) appears to be a promising route.

M.C. and E.D. acknowledge financial support from the project Light-on-Dark granted by MIUR through PRIN2017-2017K7REXT. M.S. acknowledges support from the STFC Consolidated Grant ST/V00087X/1.

Facilities: HST(ACS, WFC3).

Software: DAOPHOT IV (Stetson 1987, 1994).

Appendix Differential Reddening

We corrected the observed magnitudes for the effects of differential reddening following the same approach described in Cadelano et al. (2020c, see also Dalessandro et al. 2018a). Briefly, we selected a sample of RGBs in the F438W–F814W frame and created a mean ridge line in the magnitude range

$19.5 < m_{F438W} < 21.5$. Then we computed the distance of each one of these selected stars from the mean ridge line along the reddening vector, defined using the extinction coefficients obtained from Cardelli et al. (1989) and Girardi et al. (2002). This reference sample is used to assign a distance from the mean ridge line to all the sources in our photometric catalog, calculated as the σ clipped median of the distance values measured for the 30 closest reference stars. Finally, the resulting values of the distances can be easily converted into variation of the color excess $\delta E(B - V)$ using an adapted version of Equation (1) in Cadelano et al. (2020c). As expected due to the low average extinction and very well defined CMD sequences, we find negligible reddening variations ($\delta E(B - V) \leq 0.01$) within the surveyed field of view. Stellar magnitudes in Figure 1 are corrected for differential reddening.

ORCID iDs

Mario Cadelano <https://orcid.org/0000-0002-5038-3914>

Emanuele Dalessandro <https://orcid.org/0000-0003-4237-4601>

Maurizio Salaris <https://orcid.org/0000-0002-2744-1928>

Nate Bastian <https://orcid.org/0000-0001-5679-4215>

Alessio Mucciarelli <https://orcid.org/0000-0001-9158-8580>

Sara Saracino <https://orcid.org/0000-0003-4746-6003>

Silvia Martocchia  <https://orcid.org/0000-0001-7110-6775>
 Ivan Cabrera-Ziri  <https://orcid.org/0000-0001-9478-5731>

References

- Anderson, J., & King, I. R. 2006, PSFs, Photometry, and Astronomy for the ACS/WFC, Instrument Science Report ACS 2006-01
- Bastian, N., & de Mink, S. E. 2009, *MNRAS*, 398, L11
- Bastian, N., & Lardo, C. 2015, *MNRAS*, 453, 357
- Bastian, N., & Lardo, C. 2018, *ARA&A*, 56, 83
- Bellini, A., Anderson, J., & Bedin, L. R. 2011, *PASP*, 123, 622
- Bellini, A., & Bedin, L. R. 2009, *PASP*, 121, 1419
- Brodie, J. P., & Strader, J. 2006, *ARA&A*, 44, 193
- Cabrera-Ziri, I., Bastian, N., Longmore, S. N., et al. 2015, *MNRAS*, 448, 2224
- Cabrera-Ziri, I., Lardo, C., Davies, B., et al. 2016, *MNRAS*, 460, 1869
- Cabrera-Ziri, I., Speagle, J. S., Dalessandro, E., et al. 2020, *MNRAS*, 495, 375
- Cadelano, M., Chen, J., Pallanca, C., et al. 2020a, *ApJ*, 905, 63
- Cadelano, M., Dalessandro, E., Ferraro, F. R., et al. 2017, *ApJ*, 836, 170
- Cadelano, M., Dalessandro, E., Webb, J. J., et al. 2020b, *MNRAS*, 499, 2390
- Cadelano, M., Ferraro, F. R., Istrate, A. G., et al. 2019, *ApJ*, 875, 25
- Cadelano, M., Saracino, S., Dalessandro, E., et al. 2020c, *ApJ*, 895, 54
- Cardelli, J. A., Clayton, G. C., & Mathis, J. S. 1989, *ApJ*, 345, 245
- Carretta, E., Bragaglia, A., Gratton, R., & Lucatello, S. 2009, *A&A*, 505, 139
- Carretta, E., Bragaglia, A., Gratton, R. G., et al. 2010, *A&A*, 516, A55
- Chung, C., Yoon, S.-J., & Lee, Y.-W. 2011, *ApJL*, 740, L45
- Dalessandro, E., Cadelano, M., Vesperini, E., et al. 2018a, *ApJ*, 859, 15
- Dalessandro, E., Cadelano, M., Vesperini, E., et al. 2019, *ApJL*, 884, L24
- Dalessandro, E., Ferraro, F. R., Massari, D., et al. 2013, *ApJ*, 778, 135
- Dalessandro, E., Ferraro, F. R., Massari, D., et al. 2015, *ApJ*, 810, 40
- Dalessandro, E., Lanzoni, B., Beccari, G., et al. 2011, *ApJ*, 743, 11
- Dalessandro, E., Lapenna, E., Mucciarelli, A., et al. 2016, *ApJ*, 829, 77
- Dalessandro, E., Lardo, C., Cadelano, M., et al. 2018b, *A&A*, 618, A131
- Decressin, T., Meynet, G., Charbonnel, C., Prantzos, N., & Ekström, S. 2007, *A&A*, 464, 1029
- Denissenkov, P. A., & Hartwick, F. D. A. 2014, *MNRAS*, 437, L21
- D'Ercole, A., Vesperini, E., D'Antona, F., McMillan, S. L. W., & Recchi, S. 2008, *MNRAS*, 391, 825
- Gieles, M., Charbonnel, C., Krause, M. G. H., et al. 2018, *MNRAS*, 478, 2461
- Girardi, L., Bertelli, G., Bressan, A., et al. 2002, *A&A*, 391, 195
- Gratton, R., Bragaglia, A., Carretta, E., et al. 2019, *A&ARv*, 27, 8
- Hidalgo, S. L., Pietrinferni, A., Cassisi, S., et al. 2018, *ApJ*, 856, 125
- Horta, D., Hughes, M. E., Pfeffer, J. L., et al. 2021, *MNRAS*, 500, 4768
- Kamann, S., Bastian, N., Gossage, S., et al. 2020, *MNRAS*, 492, 2177
- Kamann, S., Bastian, N., Usher, C., Cabrera-Ziri, I., & Saracino, S. 2021, *MNRAS*, 508, 2302
- Krujsssen, J. M. D. 2015, *MNRAS*, 454, 1658
- Larsen, S. S., Brodie, J. P., Grundahl, F., & Strader, J. 2014, *ApJ*, 797, 15
- Latour, M., Husser, T. O., Giesers, B., et al. 2019, *A&A*, 631, A14
- Li, C. 2021, *ApJ*, 921, 171
- Li, C., Wang, Y., Tang, B., et al. 2020, *ApJ*, 893, 17
- Libralato, M., Bellini, A., Piotto, G., et al. 2019, *ApJ*, 873, 109
- Martocchia, S., Cabrera-Ziri, I., Lardo, C., et al. 2018, *MNRAS*, 473, 2688
- Martocchia, S., Dalessandro, E., Lardo, C., et al. 2019, *MNRAS*, 487, 5324
- Martocchia, S., Lardo, C., Rejkuba, M., et al. 2021, *MNRAS*, 505, 5389
- Massari, D., Raso, S., Libralato, M., & Bellini, A. 2021, *MNRAS*, 500, 2012
- Milone, A. P., Piotto, G., Bedin, L. R., et al. 2012, *A&A*, 540, A16
- Milone, A. P., Piotto, G., Renzini, A., et al. 2017, *MNRAS*, 464, 3636
- Mucciarelli, A., Carretta, E., Origlia, L., & Ferraro, F. R. 2008, *AJ*, 136, 375
- Mucciarelli, A., Dalessandro, E., Ferraro, F. R., Origlia, L., & Lanzoni, B. 2014, *ApJL*, 793, L6
- Mucciarelli, A., Origlia, L., & Ferraro, F. R. 2007, *AJ*, 134, 1813
- Mucciarelli, A., Origlia, L., Ferraro, F. R., & Pancino, E. 2009, *ApJL*, 695, L134
- Piotto, G., Milone, A. P., Bedin, L. R., et al. 2015, *AJ*, 149, 91
- Salaris, M., Usher, C., Martocchia, S., et al. 2020, *MNRAS*, 492, 3459
- Saracino, S., Kamann, S., Usher, C., et al. 2020a, *MNRAS*, 498, 4472
- Saracino, S., Martocchia, S., Bastian, N., et al. 2020b, *MNRAS*, 493, 6060
- Sbordone, L., Salaris, M., Weiss, A., & Cassisi, S. 2011, *A&A*, 534, A9
- Schiavon, R. P., Caldwell, N., Conroy, C., et al. 2013, *ApJL*, 776, L7
- Song, Y.-Y., Mateo, M., Bailey, J. I., III, et al. 2021, *MNRAS*, 504, 4160
- Stetson, P. B. 1987, *PASP*, 99, 191
- Stetson, P. B. 1994, *PASP*, 106, 250
- Zhang, H., de Grijs, R., Li, C., & Wu, X. 2018, *ApJ*, 853, 186